corrosion and materials degradation

MDPI

Article

Evaluating the Impact of Key Variables on Inhibitor Functionality Under Droplet Conditions

Chathumini Samarawickrama [1], Sebastian Pöhlker [2], Qiushi Deng [1,3], Paul White [1], Patrick Keil [1,2] and Ivan Cole [1,3,*]

[1] School of Engineering, RMIT University, Melbourne, VIC 3001, Australia; chathumini.sama@gmail.com (C.S.); qiushi.deng@anu.edu.au (Q.D.); patrick.keil@basf.com (P.K.)
[2] BASF Coatings GmbH, Glasuritstrasse 1, 48165 Muenster, Germany
[3] School of Engineering, College of Systems and Society, The Australian National University, Canberra, ACT 2601, Australia
* Correspondence: ivan.cole@anu.edu.au

Abstract

This study investigates droplet-induced corrosion, a localized corrosion phenomenon driven by oxygen depletion within electrolyte droplets, distinct from bulk volume corrosion. To evaluate the performance of corrosion inhibitors under droplet conditions, a rapid screening electrochemical test method was employed, using a two-electrode setup to monitor corrosion currents. The study examined systematically different exposure environments including dissolved oxygen, pH, electrolyte molarity, and droplet geometry as key factors influencing atmospheric corrosion. Results show that dissolved oxygen levels significantly affect corrosion mechanisms, while larger droplets amplify the Evans droplet effect. Importantly, effective corrosion inhibitors mitigate this effect by reducing the cathodic reaction rate in droplet conditions. These findings advance the understanding of droplet corrosion mechanisms and provide insights into designing sustainable protection strategies to improve the longevity of steel structures in aggressive environments.

Keywords: steel; zinc; droplet corrosion; atmospheric corrosion; corrosion inhibitor; pH; droplet size

1. Introduction

Structural steel is inherently at risk of atmospheric corrosion due to its exposure to moisture and oxygen, especially in coastal areas with a high chloride concentration [1–3]. The corrosion occurs when aerosols settle on metal surfaces, resulting in localized electrochemical deterioration beneath the accumulated droplets or thin films. Studies have indicated that the mechanisms of this type of corrosion differ from that in typical bulk volume electrolytes, as outlined by Evans' droplet theory [4,5]. For droplet corrosion, the corrosion rate is mainly determined by the diffusion of oxygen through the electrolyte, which can be quantified as diffusion-limited current. The form of droplets permits easier access to oxygen due to the shorter travel distance from the atmosphere to the metal surface, which accelerates corrosion reactions. According to Evan's theory, a unique phenomenon arises within the droplet: the diffusion of oxygen is not uniform across its structure. The droplet center where oxygen needs to travel a longer distance to reach the surface promotes anodic behavior, whereas cathodic behavior is often observed at the edge of the droplet for enriched oxygen by more efficient diffusion. When investigating atmospheric/droplet corrosion, it is essential to consider multiple factors, as these parameters significantly

Check for updates

Academic Editor: Daniel John Blackwood

Received: 24 November 2025
Revised: 6 February 2026
Accepted: 6 February 2026
Published: 13 February 2026

Copyright: © 2026 by the authors. Licensee MDPI, Basel, Switzerland. This article is an open access article distributed under the terms and conditions of the Creative Commons Attribution (CC BY) license.

influence the corrosion processes and mechanisms involved, such as oxygen concentration, pH gradients, droplet size and morphology, salt concentration, secondary spreading phenomena, and many others [6]. These factors should also be considered for the selection of corrosion inhibitors [6].

The dissolved oxygen content contributes to one of the leading factors distinguishing the corrosion mechanisms under a droplet versus in bulk volume. The varying cathodic and anodic sites within a droplet result in the formation of pH gradients between the droplet edge and center, which evolve over time [7]. The impact of these pH gradients on corrosion under different conditions has been extensively documented in the literature [8–10]. In the field-based atmospheric corrosion and cabinet testing scenarios, it is essential to acknowledge the diverse range of droplet sizes, which can span from 2 µL to 100 µL. This variability is dominated by intricate alterations in droplet geometry, such as the merging of neighboring droplets. When dealing with multiple interactive droplets, these modifications can result in a shift in the distribution of droplet sizes [6]. Previous studies have shown the change of oxygen concentration gradients, grain boundaries and inclusions under different aerosol and droplet sizes, casting an influence on the corrosion rate [11–13]. The aerosol smaller than a grain leads to a low corrosion rate, whereas larger droplet sizes this would cover multiple grain boundaries and inclusions, resulting in a higher corrosion rate.

Understanding how these factors influence the efficiency and behavior of corrosion inhibitors is of paramount importance. Therefore, this study focuses on investigating the factors influencing droplet corrosion. The primary objective is to comprehensively examine the effects of exposure time, dissolved oxygen content in solution, solution pH, inhibitor molarity, and droplet size on the efficacy of various inhibitors using electrochemical techniques. This investigation also builds on this foundation through the same established electrochemical testing methodology used in our previous study [7], which accommodates both bulk and droplet volumes to evaluate inhibitor performance.

2. Materials and Methods

2.1. Substrate Preparation

In this study, cold-rolled steel and zinc were selected as the primary substrates. Two identical metal specimens were prepared, each measuring 52 mm × 20 mm × 1 mm. After cleaning and drying, the samples were mounted in an epoxy mold with a diameter of 40 mm, maintaining a 10 mm gap between them. Before each electrochemical test, the exposed surfaces of the electrodes were polished sequentially with 400, 1200, and 2500 grit SiC papers to achieve a mirror-like finish, then rinsed with ethanol and dried using compressed air. The prepared samples were stored in a desiccator until testing. Both substrates were automotive-grade materials supplied by Chemetall GmbH, Frankfurt, Germany. The chemical composition is shown in Table 1.

Table 1. The composition of cold-rolled steel and zinc substrates (unit: %weight).

	Zn	Cu	Ti	Fe	Si	Mn	P	C
Zinc	99.85	0.7	0.08	-	-	-	-	-
Cold-rolled steel	-	-	-	99.46	0.03	0.4	0.03	0.08

2.2. Solution Preparation

The base corrosion medium was a 0.1 M NaCl solution made with de-ionized water. The inhibitor solutions were made with a concentration of 10 mM, mixed for at least 24 h or until fully dissolved in the chloride solution. All solutions were continuously stirred with a magnetic stirrer at ambient temperature until the inhibitors were completely dissolved or

the solution reached saturation. The initial pH of the solutions was adjusted using dilute sodium hydroxide or diluted hydrochloric acid as required to a neutral level (pH 7.0 ± 0.5) and the solution was saturated with oxygen unless specified otherwise. All used chemicals were of analytical grade.

2.3. Electrochemical Technique

The electrochemical configuration and testing approach adopted in this work were based on the procedures described in earlier studies [7]. The multi-electrode cell setup involved connecting the reference and counter electrodes to one metal specimen, while the working electrode was linked to a second specimen, both previously embedded in epoxy resin. A polarization test was then performed using a Biologic VMP300 potentiostat to evaluate the inhibitor's performance on zinc and steel.

Whilst the conventional approach permits the calculation of commonly used electrochemical parameters and efficiencies of inhibition, the proposed multielectrode system in this study (Figure 1) facilitates rapid corrosion evaluation and the investigation within artificial electrolyte shapes, i.e., droplets. Here, a voltage of 0 V is applied across two identical electrodes, one of which behaves anodically and the other cathodically. The current flow between these electrodes is influenced by the balance of anodic and cathodic surface reactions taking place. The addition of a cathodic inhibitor suppresses cathodic processes, whereas an anodic inhibitor reduces the current associated with the anodic electrode. This approach enables simultaneous evaluation of both anodic and cathodic inhibition, making it an efficient method for screening multifunctional inhibitor formulations. Furthermore, the system reaches steady state rapidly, significantly shortening the experimental duration. This reduction in testing time helps mitigate issues such as droplet evaporation, which is particularly advantageous. Additionally, the accelerated stabilization is beneficial for complex alloys with heterogeneous microstructures, as it minimizes surface alterations prior to scanning [7].

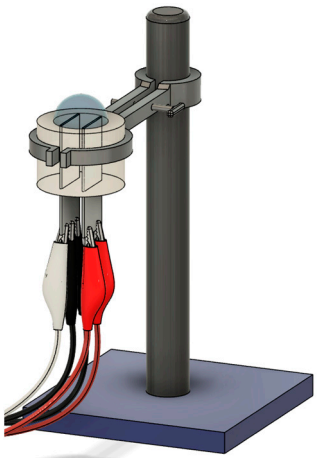


Figure 1. Schematic diagram of the electrochemical cell setup for polarization test with a single droplet.

2.3.1. Polarization Test

The experimental sequence commenced with an open-circuit potential (OCP) stabilization period lasting either 10 or 90 min. Following this, polarization measurements were performed by applying a potential of −75 mV relative to OCP for 60 s. The system was then returned to OCP for 30 s to re-establish steady-state conditions before applying a subsequent potential of +75 mV versus OCP for another 60 s. The mean current values obtained during these polarization steps were used to calculate the inhibition efficiency of the tested formulations. Unless otherwise specified, experiments employed a droplet volume of

800 µL and a bulk electrolyte volume of 80 mL, with each test repeated three times to ensure reproducibility. Averaged corrosion currents were subsequently utilized to determine the inhibition efficiency of the inhibitors under investigation. The inhibition efficiency (IE) was calculated using the following equation:

$$IE(\%) = (1 - \frac{i_{inh}}{i_{blank}}) \times 100$$

where i_{inh} and i_{blank} are current densities measured with and without the addition of inhibitor, respectively.

When active protection is provided by inhibitors, scratches or damage to the coatings can cause the corrosion inhibitors within these coatings to be released into the solution. This release helps shield the exposed metal and ensures protection. As a result, the leached inhibitors must remain active in the solution. This rationale supports conducting electrochemical tests with inhibitors in solution instead of on pre-coated metal substrates, as it better simulates real-world conditions and responses.

2.3.2. Potentiodynamic Scanning

Potentiodynamic measurements were conducted using a conventional three-electrode electrochemical cell with a bulk electrolyte volume. The configuration comprised a platinum counter electrode, a saturated Ag/AgCl reference electrode, and a platinum mesh (exposed area: 25 mm × 35 mm) alongside the metal specimen serving as the working electrode. The cell was filled with 180 mL of electrolyte solutions for all tests. Prior to polarization, the open-circuit potential (OCP) was monitored for 30 min to ensure stabilization. Subsequently, a full polarization scan was performed over a potential range of −350 mV to +350 mV relative to OCP at a scan rate of 1 mV s^{-1}. During testing, the electrolyte was continuously either aerated with compressed air or purged with nitrogen at a controlled low flow rate to establish oxygen-rich and oxygen-depleted conditions, respectively.

All experiments were carried out under ambient laboratory conditions (temperature: 22 ± 1 °C; relative humidity: ~50%) to assess inhibitor performance in both droplet and bulk environments. This methodology enabled a comprehensive evaluation of corrosion inhibition under varied atmospheric and electrolyte conditions, providing insights into the inhibitor's effectiveness across different exposure scenarios.

3. Results

3.1. Effect of Dissolved Oxygen

An experimental framework was developed to investigate the influence of dissolved oxygen on corrosion kinetics and inhibitor performance. Two distinct test environments were established: one with oxygen-saturated inhibitor solutions to represent conditions of maximum oxygen availability (droplet exposure) and another with oxygen-depleted solutions to simulate low-oxygen conditions (bulk exposure). This dual-environment approach enabled a comparative evaluation of oxygen concentration effects on inhibition mechanisms. The findings highlight the complex interplay between oxygen levels and inhibitor efficiency in mitigating corrosion, providing insight into their combined role under varying conditions. Potentiodynamic scans were performed following a 90 min OCP stabilization period using steel substrates. The saturated oxygen concentration is approx. 8.9 mg/L at lab temperature.

After analyzing the data presented in Figure 2, it is evident that there is a notable disparity in the corrosion current as a result of different oxygen levels This contrast is particularly noticeable for inhibitor 5-methyl-1,3,4-thiadiazole-2-thiol (MMTD) at pH 7 and 10. Interestingly, the effect of dissolved oxygen is minimal at pH 3 in both uninhibited and

inhibited solutions. In highly acidic environments, any surface oxides are dissolved, thereby hindering passivation. Therefore, the presence of any additional oxygen may not have any effect on the corrosion rate or inhibitor performance. At both pH 7 and pH 10, MMTD shows a more prominent passivation region in the oxygen-deprived solution as compared to the counterparts. resulting in reduced efficiency. This suggests that, while the corrosion mechanism may vary due to the abundance of oxygen in droplets, the performance of the inhibitor may or may not differ in such conditions.

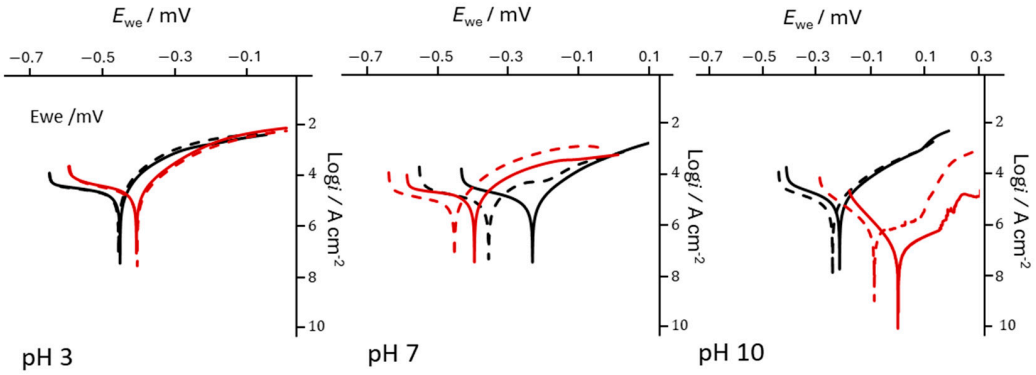


Figure 2. Potentiodynamic scanning test results using a conventional 3-electrode cell setup for selected inhibitors under oxygen-saturated (solid lines) and oxygen-deprived (broken lines) conditions, with steel at pH 3, 7 and 10. Black: without inhibitor; red: with 10 mM 5-methyl-1,3,4-thiadiazole-2-thiol.

Figure 3 shows the inhibition performance of MMTD at different pH values after 10 min (left) and 90 min (right) of immersion. In contrast to Figure 2, which presents results obtained using the conventional three-electrode setup, Figure 3 was measured using our newly developed two-electrode system to directly compare bulk and droplet electrolyte geometries. MMTD initially exhibits limited effectiveness, which improves over time, indicating that additional immersion is required for protective film formation. Importantly, the inhibition performance differs between bulk and droplet conditions even at the same oxygen concentration, highlighting that environmental factors other than oxygen also influence corrosion behavior. This demonstrates that conventional bulk measurements alone may not fully capture the inhibitor's effectiveness under realistic droplet conditions.

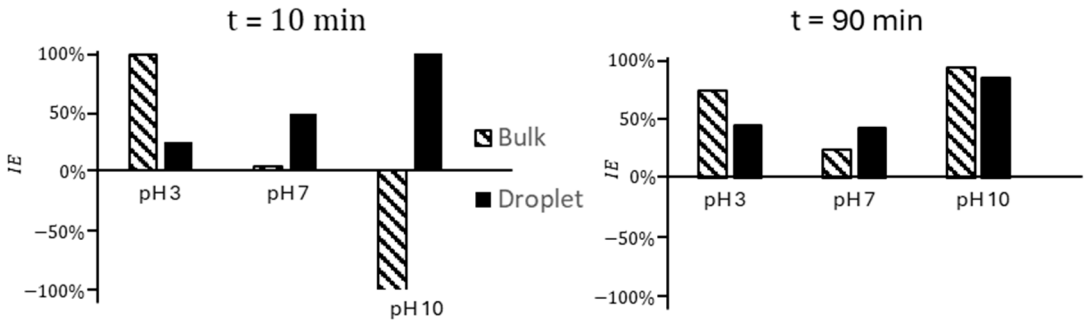


Figure 3. Comparison of inhibition efficiencies of 5-methyl-1,3,4-thiadiazole-2-thiol in bulk and droplet volumes at pH 3, 7 and 10 on steel at 10 min and 90 min of exposure. Negative IE suggests corrosion acceleration.

3.2. Effect of pH

The major work in this study relies on the rapid-screening electrochemical method proposed to analyze both droplet and bulk volumes. The droplet-on-plate tests have shown considerable variations in pH within a droplet, underscoring the importance of understanding pH fluctuations within a droplet during the polarization test [8]. As a result,

a few drops of universal indicator were included in the electrolyte before carrying out the polarization test, which is a mixture of pH-sensitive dyes that changes color depending on the pH of the solution.

The series of images in Figure 4 below illustrates changes in pH within a droplet at different polarization states. The color change near the plate may result from the production of hydroxide ions. It is observed that during cathodic polarization, greater alkalinity is shown at the plate connected to the working electrode, while the opposite trend is observed during anodic polarization. However, in the bulk volume, pH changes would be negligible. Therefore, an inhibitor that is effective at pH 7 in bulk volume may not be as effective in a droplet volume at the same pH due to the pH variation. The increase in pH at the electrodes could either cause passivation or accelerate corrosion, depending on the pH level and the nature of the substrate. Further investigation is required to understand the changes in inhibitor performance at different pH values.

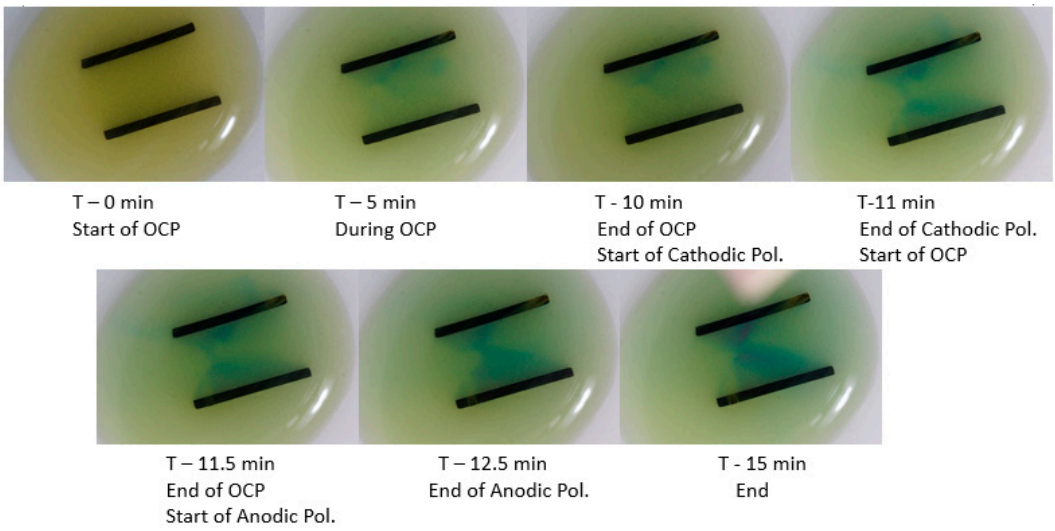


Figure 4. pH variation within an uninhibited droplet during the electrochemical test on steel (top metal plate—working electrode; bottom metal plate—ref/counter electrode). Warmer color shows local acidity; cooler color reflects local alkaline area.

Despite variations in environments, the difference in corrosion currents measured at each pH is only about 10–20%. This may be associated with reduced corrosion susceptibility and the presence of oxides, as the difference observed between the two scenarios was much more significant for steel.

A previously proposed rapid screening technique [7] was employed to assess the impact of various inhibitors on galvanized steel. Figure 5 demonstrates the effect of pH for an uninhibited droplet on a zinc surface. This was used as a baseline for evaluating the effect of pH on corrosion inhibitors.

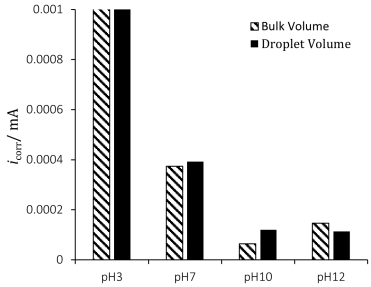


Figure 5. Corrosion current measured with an uninhibited solution for zinc under different pH conditions.

The inhibitors were maintained at a uniform concentration of 10 mM, and the assessments were conducted at varying initial pH values, specifically pH 3, 7, and 10. These evaluations were performed using both bulk and droplet volumes, and the results are visually depicted in Figure 6 below.

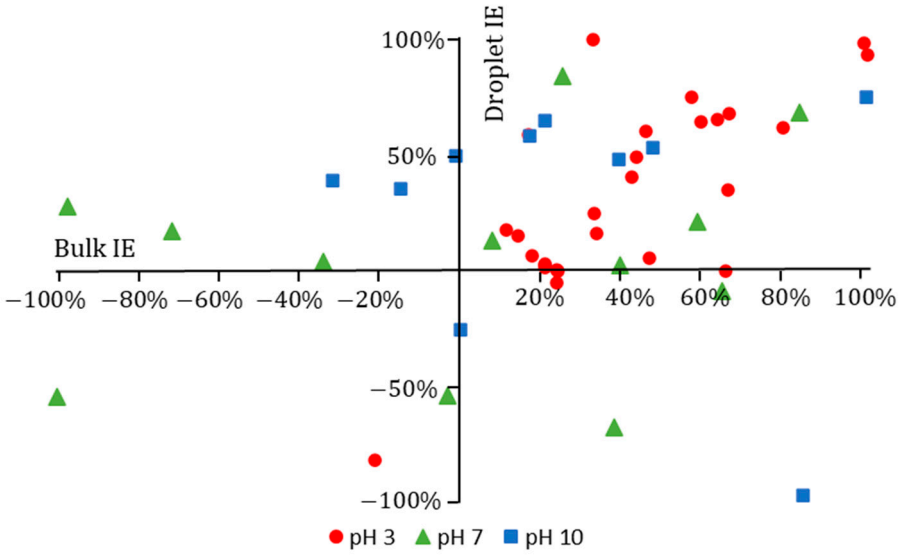


Figure 6. Comparison of inhibition efficiencies in bulk and droplet volumes at pH 3, 7 and 10 on zinc.

It is observed that most inhibitor solutions initialized at a pH of 3 follow a relatively linear trend, indicating comparable performance in both bulk and droplet volumes, with some more scattered points. It is noteworthy that most of the selected inhibitors demonstrate favorable performance within this pH range when contrasted with other initial pH values. Intriguingly, at pH 7, inhibitors display a distinctly scattered pattern, with a higher frequency of inhibitors exhibiting differentiated behavior. The results indicate that inhibitors exhibiting high efficacy in bulk environments tend to show only moderate performance in droplet conditions. As illustrated in Figure 6, several inhibitors tested at pH 10 fall outside the plotted range due to negative inhibition efficiencies, effectively acting as corrosion accelerators. Among the remaining compounds, most cluster around approximately 50% inhibition efficiency in droplet exposures, while their performance in bulk solutions varies widely, including both positive and negative values. These observations suggest that alkaline conditions (pH 10) generally enhance corrosion protection within droplet environments compared to bulk systems.

The impact of pH is extensively studied in the corrosion industry due to its crucial role in the corrosion mechanism [14,15]. Thomas et al. [16] conducted a study to explore the effects of pH in a droplet environment on zinc corrosion behavior. The study delved into the various corrosion processes influenced by different pH levels. In the pH range of 1 to 4, zinc corrosion is predominantly controlled by cathodic reactions, with the speed of corrosion determined by the kinetics of the hydrogen evolution reaction. As the pH levels range from 4 to 11, corrosion rates stabilize due to a shift in the cathodic process from hydrogen evolution to oxygen reduction. During this phase, the surface oxides on zinc are unable to effectively act as a corrosion barrier. In alkaline environments, the reaction of zinc with the surroundings leads to the formation of diverse oxides and complexes, which vary based on the local pH and potential.

The presence of pH gradient in a small, confined space can significantly impact the process of droplet corrosion [8]. Understanding how these variations affect the effectiveness of corrosion inhibitors is crucial. Unlike the gradual pH changes that occur in larger volumes, the dynamic conditions within a droplet environment can lead to the formation

of different oxide species at different locations. Electrochemical assessments of galvanized steel suggest that corrosion inhibition is increased in acidic droplets, likely due to the dissolution of oxide layers in highly acidic environments, promoting direct interactions between corrosion inhibitors and the metal surface. In the neutral pH condition, inhibitors exhibit different behavior in droplets compared to bulk volumes, with highly alkaline conditions supporting better performance. At pH 10, a passive zinc film forms according to the Pourbaix diagram, potentially serving as an effective anodic barrier. However, increased oxygen diffusion in droplets and a thin, porous precipitate layer can accelerate metal dissolution, leading to significant corrosion. Nevertheless, a thicker oxide layer forms over time, providing a more durable protective barrier [16].

To examine these variations in greater detail, Figure 7 illustrates the inhibition performance of a solution containing 10 mM 5-methyl-1,3,4-thiadiazole-2-thiol (MMTD) across different pH conditions in both bulk and droplet configurations. The plot provides a comparative assessment of inhibition efficiencies, with polarization measurements conducted following a 10 min OCP stabilization period.

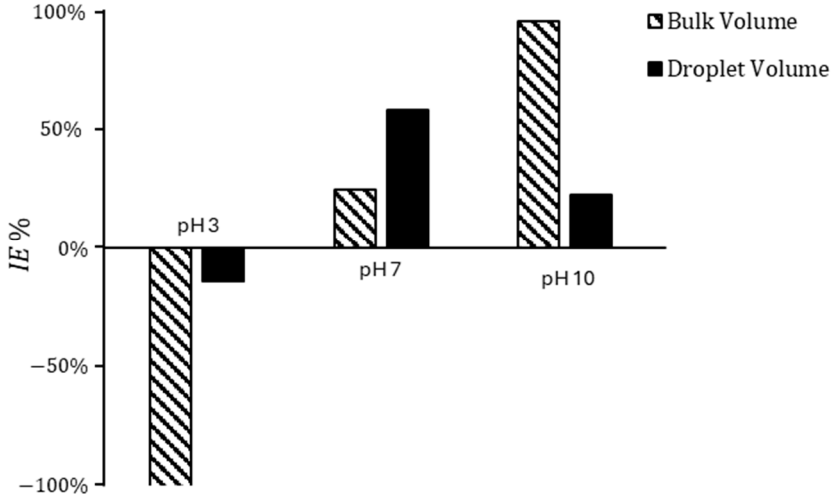


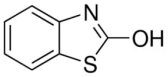
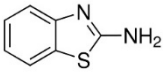
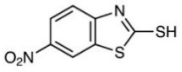
Figure 7. Comparison of inhibition efficiencies of 5-methyl-1,3,4-thiadiazole-2-thiol in bulk and droplet volumes at pH 3, 7 and 10 on zinc.

At pH 3, the inhibitor in both electrolyte conditions exhibits poor inhibition and accelerated corrosion. Conversely, under neutral conditions, the corrosion inhibitor demonstrates superior performance within droplets, while the alkaline droplet results in comparatively diminished effectiveness. Notably, at pH 10, corrosion currents measured for both inhibited and uninhibited conditions are notably lower than those observed at pH 3 and 7, potentially attributed to oxide formation. The pKa of 5-methyl-1,3,4-thiadiazole-2-thiol is 6.49, implying that at a pH below this value, protonation of the molecule happens, which may lead to a decrease in its corrosion inhibition efficiency [17]. At a higher pH value, deprotonation occurs, leading to the formation of electron lone pairs, which improves the chemical reactivity of the inhibitor molecule for better surface bonding and ensures higher inhibition efficiency. The comparison in Figure 7 also illustrates significant differences in corrosion inhibition between bulk and droplet volumes, mainly when steel is used as the substrate. This underscores the potential variations in corrosion inhibitor performance in droplet corrosion scenarios. It is worth noting that the inhibitor 5-methyl-1,3,4-thiadiazole-2-thiol is known for its effectiveness in bulk volumes. The data in this study were collected after a 10 min interval, which may account for the observed poor inhibition efficiency at neutral pH. This could be due to the film-forming nature of the corrosion inhibitor, which might require a longer time to exhibit its optimal effectiveness.

3.3. Simulation of Droplet Conditions in Full-Immersion Testing

In this study, the same corrosion inhibitor concentration is applied across bulk volume and droplet volume corrosion tests. For droplet tests, a volume of 800 µL is used, whilst for bulk volume tests, a volume of 80 mL is used (Scenario 01). The experimental approach involves the employment of electrolyte volumes that are significantly reduced, specifically to a factor 100 times lower than that of the conventional bulk volume; however, exposed metal surface is identical for both experimental conditions. This methodology focuses on the corrosion inhibition process where the number of molecules available for interaction within the droplet is significantly lower than that in the bulk volume. As a result, the limited availability of corrosion inhibitors leads to a decrease in their effectiveness over time due to their constrained presence within the droplet. Therefore, to understand whether the total amount of inhibitor molecules impacts the inhibition efficiency, a series of experiments were conducted by controlling this variable for both scenarios. The chemical details of the inhibitor used is summarized in Table 2.

Table 2. Chemical details of inhibitor molecules used for bulk and droplet tests.

2-BTOH	2-hydroxybenzothiazole	
2-ABT	2-aminobenzothiazole	
MNBT	2-mercapto-6-nitrobenzothiazole	

Accordingly, a 0.1 mM inhibitor concentration was used for full immersion testing, while a 10 mM inhibitor concentration was maintained for droplet corrosion tests (Scenario 02). The NaCl concentration for both scenarios was fixed at 0.1 M. Data from droplet volume testing is represented with dotted lines, and the equivalent bulk volume data is shown in solid lines, using consistent colors for clarity.

Despite the number of moles, droplet corrosion consistently exhibits higher corrosion current across all three tested corrosion inhibitors. This unintuitive observation indicates that a comparable number of moles in this study does not necessarily result in better performance and implies a different working mechanism for corrosion inhibitors in droplet and complete immersion testing. It should be noted that, over longer experimental times, inhibitor molecules diffuse through the bulk solution to reach the metal surface, whereas in the droplet environment, these molecules are in close proximity to the metal substrate. Noted is also that, as discussed above, oxygen availability plays a significant role in corrosion and inhibition. Notably, 2-mercapto-6-nitrobenzothiazole (MNBT) demonstrates a distinct inhibiting effect with reduced corrosion current after approximately 60 min of exposure under a droplet condition (Figure 8), implying the formation of an effective protective film. In contrast, the corrosion current in bulk solutions tends to increase over time, indicating a lack of inhibition efficacy throughout the test duration. Furthermore, even when maintaining consistent inhibitor concentration and molarity in droplet and bulk volumes, these effects are not solely attributable to molarity for this inhibitor candidate. It is also observed that, in the case of zinc, droplet tests lead to a higher corrosion current for all three corrosion inhibitors at the onset. However, at varying exposure times from 25 to 40 min, the corrosion rate in the bulk volume progressively exceeds that in the droplet tests. This could be related to the oxide formation occurring more rapidly under droplet conditions compared to full immersion testing, likely due to high oxygen availability.

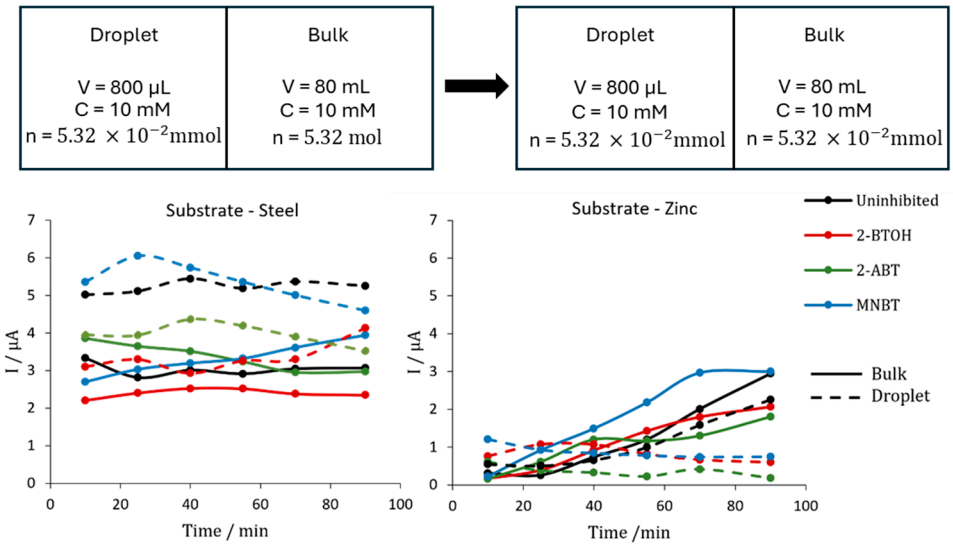


Figure 8. Effect of corrosion inhibitor molarity in droplet (broken lines) and bulk volume (solid lines) on steel (**left**) and zinc (**right**).

Nevertheless, the decrease in corrosion current over time is revealed once the inhibitor molecules interact with the metal surface in droplet environments, presumably attributed to a more stable protective film. In contrast, the full-immersion tests demonstrate that molecules such as 2-ABT and MNBT exhibit a reduced corrosion current compared to the uninhibited scenario; however, this current remains markedly higher than that observed under droplet conditions. This distinct behavior may be explained by the considerably lower number of moles in the bulk volume, which results in a slower diffusion rate of corrosion inhibitor molecules over time during the dynamic film growth at the interface, thereby affecting time-dependent corrosion protection.

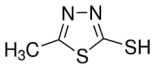
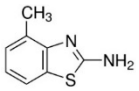
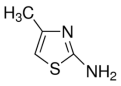
These experimental observations, shown in Figure 8, demonstrate a reduced effectiveness of corrosion inhibitors under droplet conditions compared to bulk immersion for steel. However, the efficiency of corrosion inhibitors in bulk volume is significantly lower than that observed for droplet volume. This suggests an alternative mechanism of inhibition in relation to steel substrates. However, with zinc, it appears that after a certain time period, the corrosion current measured in bulk volume surpasses that in droplet volume for the uninhibited and inhibited environments. This may suggest that corrosion under a droplet is optimal at early stages due to an abundance of dissolved oxygen. However, the transition time of oxygen to the surface, once the initial oxygen is depleted, may be slow, and the formation of an oxide layer is significantly impeded over time in bulk volumes. Unlike steel, for zinc, corrosion inhibitors seem to perform better in droplet volume than in bulk volume, which may indicate the slow diffusion of corrosion inhibitors to the metal surface.

3.4. Effect of Droplet Size

Based on our assumption that the corrosion mechanism differs significantly under a droplet compared to bulk conditions, primarily due to the shortened path for oxygen to reach the metal–electrolyte interface, variations in droplet size could influence corrosion rates [11,18,19]. To explore this concept further, a series of experiments was conducted, comparing the effects of different droplet sizes in the presence and absence of corrosion inhibitors. The same polarization test sequence outlined previously was repeated with different droplet sizes. A series of droplet sizes ranging from 200 µL to 800 µL were monitored. It was observed that over a period of 1 h, at a room temperature of 22 ± 1 °C and a relative humidity level of 55 ± 5%, the active area of the substrate remained entirely

covered by the droplet. Molecular structures of the studied inhibitors were shown in Table 3.

Table 3. Chemical information on inhibitors used in Figure 9.

MMTD	5-methyl-1,3,4-thiadiazole-2-thiol	
AMBT	2-amino-4-methylbenzothiazole	
AMT	2-amino-4-methylthiazole	

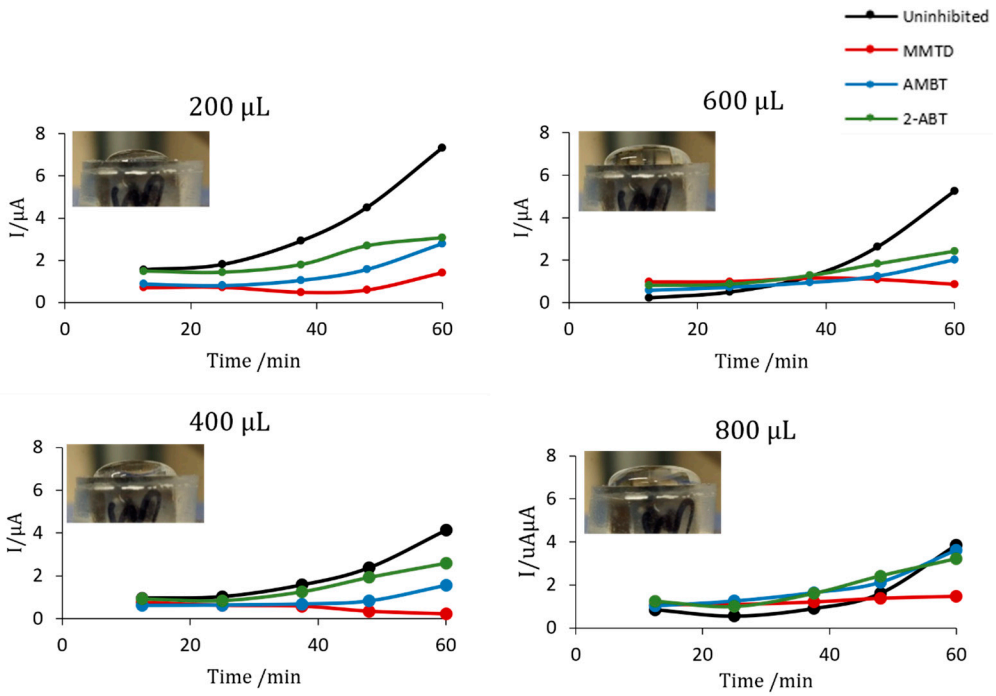


Figure 9. Effect of droplet size on the corrosion inhibitor performance over 60 min on zinc at droplet sizes ranging from 200 to 800 µL.

The plot in Figure 9 illustrates the results of these experiments. The observed variation in droplet thickness and shape across different droplet sizes can be attributed to the interplay between surface tension and gravitational forces. Smaller droplets, such as the 200 µL droplet, exhibit a more spherical shape and a smaller height due to the dominance of surface tension, which minimizes the surface area [20–24]. Larger droplets tend to flatten and spread, as seen with the 800 µL droplet, resulting in a larger diameter and a more cylindrical profile [20,25]. This is also accompanied by an increase in the contact angle, reflecting the changing balance between adhesive forces at the liquid–solid interface and cohesive forces within the liquid. As anticipated, in the case of droplets containing only NaCl, the smallest droplet size of 200 µL resulted in the highest corrosion current. Overall, this corrosion current gradually diminishes with increasing droplet size. A study conducted by E. Rahimi et al. [12] revealed that under a thick electrolyte (5 µL droplet), a two-dimensional or spherical diffusion can be considered for ORR, whereas when the droplet size is reduced to 1.5 µL, the oxygen diffusion is in a perpendicular direction to the electrode surface; i.e., planar diffusion [12]. Therefore, smaller droplets exhibit a lower concentration gradient with one-dimensional diffusion. In this setup, as the droplet

diameter is constant, the smaller droplets appear to have a higher concentration gradient than the larger droplets, as indicated below in Figure 10.

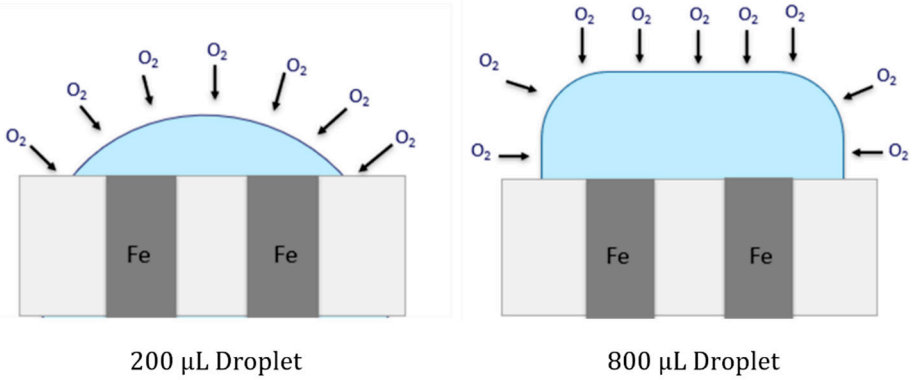


Figure 10. A schematic diagram of a (**left**) two-dimensional and (**right**) one-dimensional oxygen diffusion through the droplet on the electrochemical cell setup.

The data illustrates a clear pattern of exponentially increasing current density with longer exposure times at a consistently applied potential of +/−75 mV in relation to OCP. Interestingly, smaller droplet sizes of 200 µL and 400 µL exhibit higher current density when compared to larger droplets in the case of uninhibited droplets.

When considering variations between repeats, the data shows that smaller droplets, such as 200 µL and 400 µL, exhibit a significantly higher variation, whereas larger droplets show minimal variation. This difference can be attributed to factors such as secondary spreading, corrosion product deposition, and evaporation, which increase as the droplet size decreases [10,26]. It is important to note that the active area of the metal remains constant for each droplet size, indicating that the corrosion products formed would be similar. However, the deposition of corrosion products per unit volume decreases for larger droplet sizes, potentially impacting the variability of the current data [27]. In addition, the impact of evaporation over time on smaller droplets could be more significant compared to larger droplets [12,23,28].

As shown in Figure 11, a notable observation arises upon introducing the corrosion inhibitor: the largest droplet size measured at 800 µL exhibits an increased corrosion current, deviating from the anticipated pattern. Moreover, with regard to molecules MMTD and AMBT, a droplet size of 600 µL manifests heightened corrosion current. This indicates that a droplet size of 600 µL demonstrates relatively superior efficacy in inhibiting corrosion compared to that of an 800 µL droplet and also surpasses the performance seen at droplet sizes of 200 µL and 400 µL. Such anomalies may be associated with a more pronounced influence of factors such as evaporation rates, the formation of corrosion products, or the concentration of dissolved oxygen within the solution.

The theoretical framework suggests that smaller droplet configurations should induce higher corrosion currents, which are expected to decrease with increasing droplet size due to longer oxygen diffusion paths and reduced mass transport to the metal surface. Conversely, when sufficiently small droplets are distributed across the entire metal surface, they coalesce to form a thin electrolyte film rather than discrete droplets, resulting in a distinct corrosion regime that differs from that of isolated droplets [23]. This deviation indicates that the classical Evans droplet model may have limited applicability under these conditions, since a near-uniform electrolyte thickness across the droplet minimizes the formation of oxygen concentration gradients central to the theory. In support of this interpretation, the experimental data demonstrate that larger droplets, especially

600 µL droplets, often produce higher corrosion currents, suggesting that the geometric characteristics of larger droplets can promote more sustained corrosion activity.

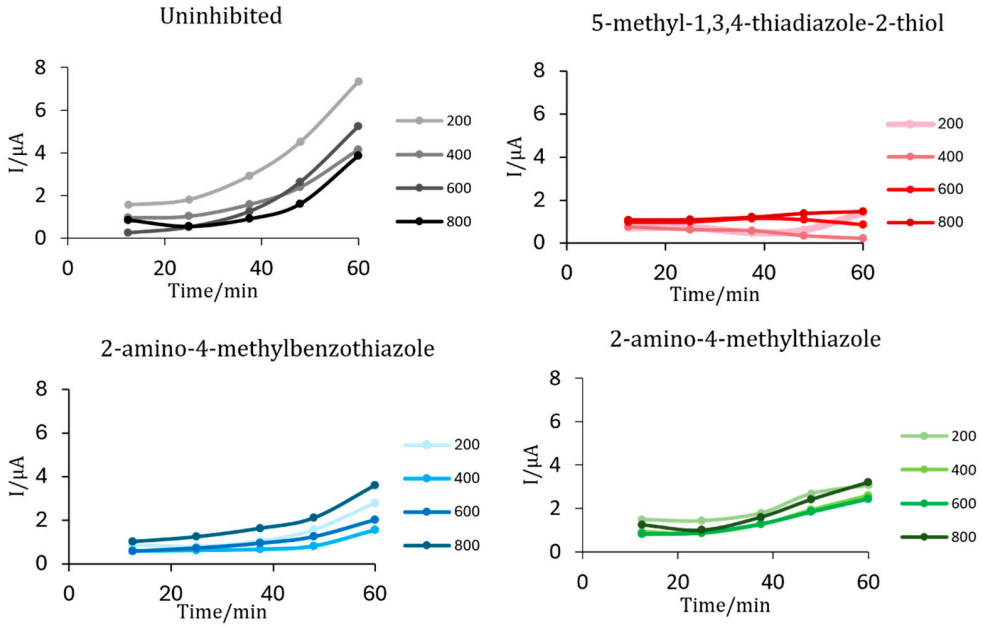


Figure 11. Effect of droplet size on the corrosion inhibitor performance over 60 min on zinc.

To accommodate the experimental investigation of smaller droplets and aerosol sizes in the range of 2–10 µL, modifications in the electrochemical cell setup are proposed, including the reduction in the exposed metal surface area. This adaptation, coupled with conducting experiments within a humidity chamber equipped to regulate humidity and temperature, aims to mitigate evaporative effects during the experimental period. Previous studies have demonstrated the effects of inclusions and grain boundaries on the metal surface for smaller droplets compared to larger droplets [18,19]. If droplet or aerosol size is smaller than the grain size, the corrosion rate is significantly reduced. However, this theory is not applicable here with reducing droplet sizes as the metal-exposed area remains constant, while the droplet's height and contact angle change [11,12].

Based on our testing method, a droplet volume spectrum spanning from 100 µL to 800 µL has been selected to ensure comprehensive coverage of the metal surface area, thereby minimizing the potential impact of evaporation phenomena on the experiment. Although the aerosol formation over the metal surface due to condensation is much smaller than that used in this test method, these droplet sizes could still represent atmospheric corrosion under rain droplets, which are known to be approximately 2 mm in diameter.

A droplet-based model was previously developed to characterize potential distribution, anodic and cathodic sites, and the spatial variation of ion and oxygen concentrations within the electrolyte and at the metal interface as a function of droplet size [29]. The oxygen concentration inside the droplet can be expressed in terms of the dimensionless ratio $\frac{kR}{D}$, where k denotes the cathodic reaction rate constant, R represents the droplet radius, and D is the diffusion coefficient of dissolved oxygen. The porosity of zinc oxide is approximately 0.276.

At a droplet size of 3–5 mm, the $\frac{kR}{D}$ value falls between the theoretical curves of $\frac{kR}{D} = 0.1$ and $\frac{kR}{D} = 1.0$. When $\frac{kR}{D} = 1$, the Evans effect becomes dominant, whereas its influence is negligible at values below 0.1. This positioning indicates a moderate contribution of Evans droplet theory for a droplet radius of approximately 5 mm [29].

As droplet size increases, the gradient in oxygen concentration within the electrolyte becomes more pronounced. In the presence of efficient corrosion inhibitors, the cathodic

reaction rate is expected to decrease, which reduces the value of k and consequently lowers the $\frac{kR}{D}$ ratio. This reduction suggests that the significance of the Evans effect diminishes when effective inhibitors are present.

Furthermore, it is pivotal that smaller droplets inherently contain fewer corrosion inhibitor molecules, thereby compromising the formation and stability of a protective film to inhibit corrosion efficaciously. In addition, it warrants consideration that larger droplets, by virtue their size, contain a higher content of dissolved oxygen relative to smaller droplets for an equivalent active area. This abundance of dissolved oxygen is believed to accelerate the corrosion process. Moreover, the phenomenon of evaporation leads to a significant increase in the concentration of corrosion inhibitors and saline solution, potentially exerting a greater influence on the corrosion rate than the presence of dissolved oxygen [4,28].

The research conducted in this study has extensively investigated various factors that influence atmospheric corrosion and how these factors impact the effectiveness of corrosion inhibitors in droplet volume when compared to bulk volume. Factors such as the presence of dissolved oxygen, pH levels, number of moles, duration of exposure, evaporation, and droplet size have been shown to significantly influence corrosion within droplet volumes, while their impact on bulk volume corrosion is less pronounced. Any alterations occurring within a droplet substantially impact the corrosion process due to the confined volume and specific environmental conditions. This research marks a significant step forward in understanding the operational mechanisms of corrosion inhibitors within droplets and highlights the distinctions between conventional immersion tests and bulk volume corrosion. It is crucial to address atmospheric corrosion precisely and identify suitable corrosion inhibitors specifically tailored for corrosion within droplets. This approach could ensure that protective coatings perform as expected, leading to more sustainable and cost-effective solutions.

4. Conclusions

This study systematically investigated the key factors affecting droplet corrosion mechanisms and the performance of corrosion inhibitors under both droplet and bulk volume conditions. It is revealed that oxygen availability strongly influences corrosion rates and inhibitor effectiveness, with higher dissolved oxygen generally accelerating corrosion. Some inhibitors were highly dependent on oxygen levels, while others were minimally affected. Corrosion inhibitor efficacy varied across pH levels due to protonation and deprotonation processes, affecting mechanisms differently in droplet versus bulk environments. For example, Zn showed varying inhibition efficiencies at pH 7 and 10, but consistent performance at pH 3 in both conditions. Rapid pH shifts within droplets also altered corrosion and inhibition dynamics, a phenomenon not observed in bulk volumes. Selected corrosion inhibitors maintained effective performance in bulk volumes even with reduced mole numbers, particularly on steel, whereas zinc showed increasing corrosion current in full-immersion tests but more stable inhibition in droplet conditions. Droplet size impacted corrosion behavior: larger uninhibited droplets exhibited reduced corrosion current, likely due to geometric variations and a more pronounced Evans droplet effect. However, the presence of effective inhibitors mitigated this effect, especially in droplet conditions.

This work highlights the distinct influences of oxygen content, pH, inhibitor concentration, droplet size, and the Evans droplet effect on corrosion mechanisms, specifically contrasting droplet and bulk volume environments. The study provides new insights into how pH changes and droplet geometry affect local corrosion and inhibition dynamics, which have been less explored in previous research. These findings offer guidance for tailoring corrosion protection strategies in atmospheric environments, emphasizing that inhibitor selection and deployment must account for both local droplet conditions and bulk

immersion scenarios. Understanding the differential behavior of inhibitors under varying oxygen and pH conditions can improve the design of corrosion mitigation measures in real-world applications.

Author Contributions: C.S.: Conceptualization, Methodology, Data Curation, Formal Analysis, Investigation, Visualization, Writing—original draft preparation. S.P.: Data Curation. Q.D.: Visualization, Writing—Review and editing. P.W.: Supervision, Writing—Review and editing. P.K.: Supervision, Funding acquisition, Conceptualization, Writing—Review and editing. I.C.: Supervision, Funding acquisition, Conceptualization, Writing—Review and editing. All authors have read and agreed to the published version of the manuscript.

Funding: This research received no external funding.

Data Availability Statement: The data presented in this study are available on request from the corresponding author.

Acknowledgments: We acknowledge Milan J Patel (RMIT University) for teaching programming principles and coding underlying data curation. The facilities and technical support of RMIT Microscopy & Microanalysis Facilities (RMMF) were acknowledged.

Conflicts of Interest: Authors Sebastian Pöhlker and Patrick Keil were employed by the company BASF Coatings GmbH (Germany). The remaining authors declare that the research was conducted in the absence of any commercial or financial relationships that could be construed as a potential conflict of interest.

References

1. Di Sarno, L.; Majidian, A.; Karagiannakis, G. The Effect of Atmospheric Corrosion on Steel Structures: A State-of-the-Art and Case-Study. *Buildings* **2021**, *11*, 571. [CrossRef]
2. Sun, C.; Kong, G.; Zhao, C.; Liu, Z.; Xu, X. Accelerated corrosion behavior of a Stellite 6 alloy in a simulated marine atmospheric environment. *J. Mater. Res. Technol.* **2026**, *40*, 1486–1499. [CrossRef]
3. Su, Y.; Wu, W.; Li, Q.; Xu, S.; Xia, X.; Zhang, J. Electrochemical corrosion behavior of aluminum conductor under current-carrying condition in a simulated atmospheric environment. *Anti-Corros. Methods Mater.* **2025**, *72*, 872–881. [CrossRef]
4. Morton, S.C.; Frankel, G.S. Atmospheric pitting corrosion of AA7075-T6 under evaporating droplets with and without inhibitors. *Mater. Corros.* **2014**, *65*, 351–361. [CrossRef]
5. Dubuisson, E.; Lavie, P.; Dalard, F.; Caire, J.-P.; Szunerits, S. Study of the atmospheric corrosion of galvanised steel in a micrometric electrolytic droplet. *Electrochem. Commun.* **2006**, *8*, 911–915. [CrossRef]
6. Zhang, K.; Rahimi, E.; Van den Steen, N.; Terryn, H.; Mol, A.; Gonzalez-Garcia, Y. Monitoring atmospheric corrosion under multi-droplet conditions by electrical resistance sensor measurement. *Corros. Sci.* **2024**, *236*, 112271. Correction in *Corros. Sci.* **2024**, *240*, 112425. [CrossRef]
7. Samarawickrama, C.; Chen, X.; White, P.; Keil, P.; Cole, I. An insight to the factors influencing corrosion under a droplet on steel and galvanised steel. In *Proceedings of the Corrosion & Prevention, 12–15 November 2023*; The Australasian Corrosion Association Ltd.: Perth, Australia, 2023.
8. Azmat, N.S.; Ralston, K.D.; Muddle, B.C.; Cole, I.S. Corrosion of Zn under acidified marine droplets. *Corros. Sci.* **2011**, *53*, 1604–1615. [CrossRef]
9. García, S.; Muster, T.; Özkanat, Ö.; Sherman, N.; Hughes, A.; Terryn, H.; De Wit, J.; Mol, J. The influence of pH on corrosion inhibitor selection for 2024-T3 aluminium alloy assessed by high-throughput multielectrode and potentiodynamic testing. *Electrochim. Acta* **2010**, *55*, 2457–2465. [CrossRef]
10. King, P.C.; Cole, I.S.; Corrigan, P.A.; Hughes, A.E.; Muster, T.H. FIB/SEM study of AA2024 corrosion under a seawater drop: Part I. *Corros. Sci.* **2011**, *53*, 1086–1096. [CrossRef]
11. Risteen, B.E.; Schindelholz, E.; Kelly, R.G. Marine Aerosol Drop Size Effects on the Corrosion Behavior of Plain Carbon Steel. *ECS Trans.* **2014**, *58*, 1. [CrossRef]
12. Rahimi, E.; Zhang, K.; Kosari, A.; Van den Steen, N.; Homborg, A.; Terryn, H.; Mol, A.; Gonzalez-Garcia, Y. Atmospheric corrosion of iron under a single droplet: A new systematic multi-electrochemical approach. *Corros. Sci.* **2024**, *235*, 112171. [CrossRef]
13. Curtin, T.; Adey, R.; Peratta, A.; Butchers, R.; Friedersdorf, F.; Agnew, L. Using Galvanic Modeling and Aerosol Spray Testing to Understand How Changes in Salt Loading Can Impact Atmospheric Corrosion. In Proceedings of the AMPP CORROSION, Denver, CO, USA, 19–23 March 2023; p. AMPP–2023–18961.

14. Pirhady Tavandashti, N.; Ghorbani, M.; Shojaei, A.; Gonzalez-Garcia, Y.; Terryn, H.; Mol, J.M.C. pH responsive Ce(III) loaded polyaniline nanofibers for self-healing corrosion protection of AA2024-T3. *Prog. Org. Coat.* **2016**, *99*, 197–209. [CrossRef]
15. Salles, R.C.M.; de Oliveira, G.C.G.; Díaz, S.L.; Barcia, O.E.; Mattos, O.R. Electrodeposition of Zn in acid sulphate solutions: pH effects. *Electrochim. Acta* **2011**, *56*, 7931–7939. [CrossRef]
16. Thomas, S.; Birbilis, N.; Venkatraman, M.; Cole, I. Corrosion of zinc as a function of pH. *Corrosion* **2012**, *68*, 015009-1–015009-9. [CrossRef]
17. 2-Mercapto-5-methyl-1,3,4-thiadiazole. In *CAS Database List*; Chemical Book: Beijing, China, 2023.
18. Li, S.; Hihara, L.H. Atmospheric-Corrosion Electrochemistry of NaCl Droplets on Carbon Steel. *J. Electrochem. Soc.* **2012**, *159*, C461. [CrossRef]
19. Tang, X.; Ma, C.R.; Orazem, M.E.; You, C.; Li, Y. Local electrochemical characteristics of pure iron under a saline droplet I: Effect of droplet size on electrochemical distribution. *Electrochim. Acta* **2020**, *354*, 136633. [CrossRef]
20. Behera, S.K.; Kumar, P.A.; Dogra, N.; Nosonovsky, M.; Rohatgi, P. Effect of Microstructure on Contact Angle and Corrosion of Ductile Iron: Iron–Graphite Composite. *Langmuir* **2019**, *35*, 16120–16129. [CrossRef] [PubMed]
21. McMurray, H.N.; Williams, G.; Cooze, N. Corrosion Driven Drying Phenomena Occurring during the Atmospheric Corrosion of Magnesium Containing Galvanized Steel. *ECS Meet. Abstr.* **2018**, *MA2018-02*, 622. [CrossRef]
22. Mohamed, A.M.A.; Abdullah, A.M.; Younan, N.A. Corrosion behavior of superhydrophobic surfaces: A review. *Arab. J. Chem.* **2015**, *8*, 749–765. [CrossRef]
23. Misyura, S.Y.; Morozov, V.S.; Orlova, E.G.; Andryushchenko, V.A. Wetting, droplet evaporation and corrosion behavior of various composite and textured materials. *Ceram. Int.* **2024**, *50*, 19269–19282. [CrossRef]
24. Huhtamäki, T.; Tian, X.; Korhonen, J.T.; Ras, R.H.A. Surface-wetting characterization using contact-angle measurements. *Nat. Protoc.* **2018**, *13*, 1521–1538. Erratum in *Nat. Protoc.* **2019**, *14*, 2259. [CrossRef] [PubMed]
25. Muster, T.H.; Bradbury, A.; Trinchi, A.; Cole, I.S.; Markley, T.; Lau, D.; Dligatch, S.; Bendavid, A.; Martin, P. The atmospheric corrosion of zinc: The effects of salt concentration, droplet size and droplet shape. *Electrochim. Acta* **2011**, *56*, 1866–1873. [CrossRef]
26. Persson, D.; Thierry, D.; Karlsson, O. Corrosion and corrosion products of hot dipped galvanized steel during long term atmospheric exposure at different sites world-wide. *Corros. Sci.* **2017**, *126*, 152–165. [CrossRef]
27. Ren, C.; Ma, L.; Luo, X.; Dong, C.; Gui, T.; Wang, B.; Li, X.; Zhang, D. High-throughput assessment of corrosion inhibitor mixtures on carbon steel via droplet microarray. *Corros. Sci.* **2023**, *213*, 110967. [CrossRef]
28. Thomson, M.; Frankel, G. Atmospheric Pitting Corrosion Studies of AA7075-T6 Under Electrolyte Droplets: Part I. Effects of Droplet Size, Concentration, Composition, and Sample Aging. *J. Electrochem. Soc.* **2017**, *164*, C653–C663. [CrossRef]
29. Cole, I.S.; Muster, T.H.; Azmat, N.S.; Venkatraman, M.S.; Cook, A. Multiscale modelling of the corrosion of metals under atmospheric corrosion. *Electrochim. Acta* **2011**, *56*, 1856–1865. [CrossRef]

Disclaimer/Publisher's Note: The statements, opinions and data contained in all publications are solely those of the individual author(s) and contributor(s) and not of MDPI and/or the editor(s). MDPI and/or the editor(s) disclaim responsibility for any injury to people or property resulting from any ideas, methods, instructions or products referred to in the content.